Applied Catalysis A: General 467 (2013) 117–123

Contents lists available at ScienceDirect

Applied Catalysis A: General

journal homepage: www.elsevier.com/locate/apcata

Liquid-phase catalytic oxidation of *p*-chlorotoluene to *p*-chlorobenzaldehyde over manganese oxide octahedral molecular sieves

Yi-Qiang Deng[a], Teng Zhang[a], Chak-Tong Au[a,b], Shuang-Feng Yin[a,*]

[a] State Key Laboratory of Chemo/Biosensing and Chemometrics, College of Chemistry and Chemical Engineering, Hunan University, Changsha 410082, Hunan, China
[b] Department of Chemistry, Hong Kong Baptist University, Kowloon Tong, Hong Kong

ARTICLE INFO

Article history:
Received 27 February 2013
Received in revised form 16 June 2013
Accepted 8 July 2013
Available online 17 July 2013

Keywords:
Manganese oxide
OMS-2
p-Chlorotoluene
p-Chlorobenzaldehyde
Catalytic oxidation
Lattice oxygen

ABSTRACT

Manganese oxide octahedral molecular sieves (OMS-2) show much higher catalytic activities in the liquid-phase catalytic oxidation of *p*-chlorotoluene than MnO_2, Mn_3O_4, $Mn(OAc)_2$ as well as than some other transition metal oxides such as Co_2O_3, V_2O_5 and Fe_2O_3. Based on temperature-programmed desorption and thermogravimetric results, it is deduced that the catalytic activity of OMS-2 can be ascribed to the abundance and mobility of lattice oxygen. We investigated the effects of reaction temperature, reaction time, catalyst amount, and initial water amount on the reaction. Under optimal reaction conditions, *p*-chlorotoluene conversion and *p*-chlorobenzaldehyde selectivity are respectively 86.0% and 68.7%. The catalysts can be easily recovered by centrifugation, and reused. According to the results of X-ray diffraction and N_2 adsorption/desorption analyses, there is no significant change in major characteristics of the catalyst after 4 cycles of reaction.

1. Introduction

The selective oxidation of *p*-chlorotoluene to *p*-chlorobenzaldehyde is important because *p*-chlorobenzaldehyde is an essential intermediate in the production of dyes, pharmaceutical drugs, optical brighteners, and agricultural chemicals [1]. The commercial production of *p*-chlorobenzal chloride is mainly by side-chain chlorination of *p*-chlorotoluene followed by acid hydrolysis [2]. The classical method to produce aromatic aldehyde involves multi-steps that are conducted non-catalytically in liquid phase, and falls short of the principle of sustainable chemistry [3]. In industry, soluble acetates of transition metals are used as catalysts but both conversion and selectivity are unsatisfactory. Furthermore, some of the processes are polluting and expensive mainly because the separation of soluble catalyst is always tedious and costly [4,5].

Since solid catalysts have advantages over soluble catalysts in terms of recovery and stability, efforts are put in to develop heterogeneous catalysts for the generation of aromatic aldehydes by selective oxidation of alkylaromatic hydrocarbons in gas phase (with O_2) or in liquid phase (with H_2O_2 or O_2). For example, 28% of *p*-chlorotoluene was converted to *p*-chlorobenzaldehyde with 61.6% selectivity at 325 °C using gas-phase O_2 over Fe/Mo/borosilicate molecular sieves [6], similar values (25% conversion and 66% selectivity) at 400 °C was reported in a US patent when $VCs_{0.5}FeO_x$ was used as catalyst [7]. Likewise, Bautista et al. described the preparation, structural and acid characterization of vanadium oxides supported on TiO_2-sepiolite and sepiolite, as well as their behavior in selective oxidation of chloro- and methoxy-substituted toluenes [8,9], and obtained 13% *p*-chlorobenzaldehyde yields when TiO_2-sepiolite supported vanadium oxides were used as catalysts [3]. On the other hand, it is easy to operate liquid-phase oxidation and to achieve high selectivity under relatively mild reaction conditions. Using H_2O_2 as oxidants and vanadium silicate molecular sieves as catalyst, Singh and Selvam observed *p*-chlorotoluene conversion of 13.4% and *p*-chlorobenzaldehyde selectivity of 65.0% [10]. It was reported that similar *p*-chlorobenzaldehyde selectivity could be attained over a supported Co(II) catalyst together with a supported *N*-hydroxyphthalimide promoter [11], but the conversion of *p*-chlorotoluene was only 11.0%. In these cases, the initial oxidation products are often more susceptible to oxidation than the starting material. Once a methyl group is attacked, it is likely to be oxidized to carboxylic acid. While such reactions readily give *p*-chlorobenzoic acids in high yields, it is rather difficult to stop the

* Corresponding author. Tel.: +86 731 88821171; fax: +86 731 88821171.
E-mail address: sf_yin@hnu.edu.cn (S.-F. Yin).

0926-860X/$ – see front matter © 2013 Elsevier B.V. All rights reserved.
http://dx.doi.org/10.1016/j.apcata.2013.07.015

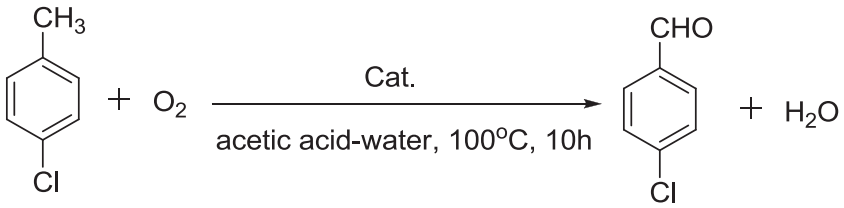

Scheme 1. Liquid-phase catalytic oxidation of *p*-chlorotoluene with O_2 over OMS-2.

reactions at the aldehyde stage. To convert *p*-chlorotoluene catalytically giving aldehyde as the main product (i.e. with high aldehyde selectivity) using various oxidants is a big challenge, and it is still an attractive research area [3].

With special electronic configurations and being variable in valence state, transition metal oxides show high catalytic activity for selective oxidation of hydrocarbons [12,13]. Manganese oxide is technologically important in catalytic and electrochemical industries [14,15]. Nanoscale manganese oxide octahedral molecular sieve (OMS-2) is a prominent oxidation catalyst under thermal conditions [16]. It has a 2×2 tunnel structure and has a chemical composition of KMn_8O_{16}, with charge-balancing K^+ ions and H_2O residing in the tunnels [17]. Such structure leads to interesting physicochemical properties such as porosity and high adsorption capacity that are commonly related to good catalytic performance [17]. The unique redox activity of OMS-2 is attributed to the presence of Mn^{3+} and Mn^{4+} ions, the long and open structure, and the formation of OH groups on the surface [18].

In this paper, we report for the first time the liquid-phase catalytic oxidation of *p*-chlorotoluene to *p*-chlorobenzaldehyde with O_2 in a reflux system using manganese oxide octahedral molecular sieve as catalyst and hydrogen bromide as reaction initiator (see Scheme 1). Adopting this atmospheric system, we achieve high *p*-chlorotoluene conversion (86.0%) and good *p*-chlorobenzaldehyde selectivity (68.7%). We believe that the process is practical for the conversion of aromatic hydrocarbons to the corresponding aldehydes using O_2 as oxidant.

2. Experimental

2.1. Materials

The chemical reagents were of analytical grade and were used without further purification. No impurities were found in *p*-chlorotoluene by GC analysis. Pure gaseous O_2 was used as the oxygen source.

2.2. Catalyst preparation

OMS-2 was prepared by refluxing a mixture of potassium permanganate and manganese sulfate in an acidic medium according to procedures described by Makwana et al. [19]. A 0.4 M solution of $KMnO_4$ (6.5 g in 113 mL of deionized water) was added to a mixture of a 1.75 M solution of $MnSO_4{\cdot}H_2O$ (9.9 g in 34 mL of deionized water) and 3.4 mL of concentrated HNO_3 (68 wt%). The resulting solution with black precipitate was stirred vigorously (600 rpm) and subject to reflux at 100 °C for 24 h. Then the precipitate was filtered out and washed with deionized water until neutral pH and dried overnight at 110 °C.

2.3. Catalyst characterization

Powder X-ray diffraction (XRD) experiment was conducted on a Bruker D8 Advance diffractometer using Cu Kα radiation. The data were recorded at a scan rate of 0.02° $(2\theta)\,s^{-1}$ in the 5–60° range. The surface area of OMS-2 was measured by the Brunauer–Emmett–Teller (BET) method on a Tristar 3000 instrument; before each measurement, the sample was heated to 300 °C and kept at this temperature for 5 h. The BET specific surface area (S_{BET}) was calculated from the adsorption data in the relative pressure range of 0.04–0.20. External surface area (S_{EXT}) was estimated by the *t*-plot method [20]. Thermal stability of catalysts was studied by means of thermogravimetric analysis (TGA, PerkinElmer Diamond TG/DTA instrument) with ca. 10 mg of sample being heated from 30 to 850 °C (ramp rate = 10 °C/min) under a N_2 atmosphere. H_2 temperature-programmed reduction (H_2-TPR) and temperature-programmed desorption of O_2 (TPD-O_2) experiments were conducted over a Micromeritics 2920 II apparatus using a thermal conductivity detector (TCD). For TPD-O_2, a catalyst (100 mg) was heated in He flow (20 mL/min) at a rate of 10 °C/min from 50 to 900 °C. Before TPD-O_2 analysis, the catalyst was degassed in He flow for 2 h. H_2-TPR experiment was carried out with the sample kept under a 20 mL/min flow of 10% H_2 in Ar. The temperature was increased from 50 to 800 °C (10 °C/min). A cold trap was installed before the TCD to stop H_2O interference.

2.4. Catalytic reactions

All experiments were carried out in a three-necked round-bottom flask equipped with a reflux condenser. Oxygen was introduced into the solution at atmospheric pressure at a desired flow rate, and the flask was placed in an isothermal paraffin oil bath with a magnetic stirrer. In a typical reaction, 1 mL *p*-chlorotoluene, 2 mL hydrobromic acid–water mixture, 10 mL acetic acid (as solvent), and 50 mg catalyst were place in the flask. The OMS-2 catalyst was heated at 110 °C overnight before being used. With stirring, the reaction system was heated to a desired temperature. Then oxygen (50 mL/min) was introduced into the bottom of the reaction mixture. After the reaction was over, the catalyst was removed by means of centrifugation, and the products were dissolved in acetonitrile and analyzed by gas chromatography (GC). To find out whether there was leaching of catalyst into the solution, the solid substance was removed after 4 h of reaction by centrifugation, and the reaction was allowed to continue for another 10 h. The products were identified by a Shimadzu GCMS-QP2010 ultra mass spectrometer and quantified by Shimadzu GC2014 chromatograph equipped with a SFID1 detector and a RTX-1 capillary column (30 m × 0.25 mm × 0.25 μm). The internal standard method was employed with biphenyl being the internal standard. The outlet gases were also analyzed on an Agilent 6890 N GC with TCD and Agilent GS-GASPRO capillary column (30 m × 0.32 mm × 0.25 μm). We detected no formation of gas products.

3. Results and discussion

3.1. Catalyst characterization

The XRD patterns of as-synthesized and used (four times) OMS-2 are shown in Fig. 1 The OMS-2 exhibits a pattern of tetragonal cryptomelane-type corresponding to KMn_8O_{16} (JCPDS 29-1020).

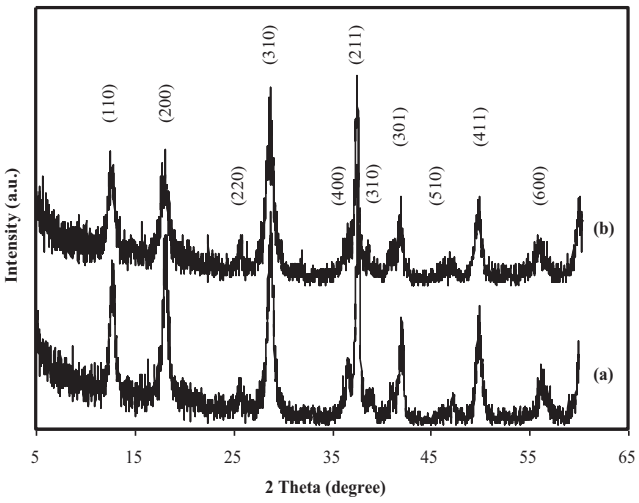

Fig. 1. X-ray diffraction patterns of (a) fresh OMS-2, and (b) used (4 cycles) OMS-2.

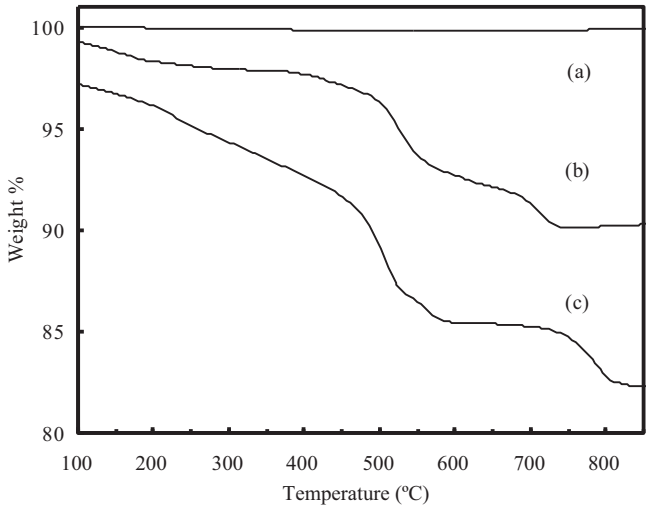

Fig. 2. TGA profiles of (a) commercial Mn_3O_4, (b) OMS-2, and (c) commercial MnO_2.

There is no obvious difference between the patterns of the fresh and used catalysts. It is hence deduced that there is no change in catalyst structure during the reaction. Furthermore, there is no impurity phase observed over the two samples. The scanning electron micrographs of fresh and used catalyst show a fibrous needle-like morphology, typical of OMS-2 materials (Fig. S1).

Listed in Table 1 are the textural properties of the nanomaterials. The BET surface area of fresh OMS-2 is 71.8 m^2/g, slightly higher than that of used catalyst (70.5 m^2/g). The S_{EXT} values are very close to the S_{BET} values, indicating that the measured surface area is predominantly external. The micropore volume of the materials only contributes to less than 1% of the total pore volume. It is noted that similar findings were reported by Tang et al. [21] and Luo et al. [22]. According to the adsorption isotherms of adsorbates reported by Wang et al. [23], the average crystalline pore openings of cryptomelane materials is about 0.46 nm. Nonetheless, it is plausible that the effective pore openings of the material are in the range of 0.265–0.330 nm. It is known that the dynamic diameter of N_2 is 0.326 nm. In other words, a great majority of N_2 are not adsorbed inside the microporous tunnels of cryptomelane.

The lattice oxygen content of OMS-2 was studied by thermogravimetric analysis. Fig. 2 shows the TGA curves of commercial Mn_3O_4, OMS-2, and commercial MnO_2. Generally, weight losses of this kind in the 30–850 °C range can be divided into four categories: (I) 30–200 °C attributable to desorption of physisorbed water, (II) 200–400 °C attributable to desorption of chemisorbed water and oxygen, (III) 400–680 °C ascribable to release of lattice oxygen in the "$MnO_2 \rightarrow Mn_2O_3$" process, and (IV) 680–850 °C ascribable to the evolution of O_2 in the "$Mn_2O_3 \rightarrow Mn_3O_4$" process [24,25]. As shown in Fig. 2a, Mn_3O_4 only displays a small weight loss (about 0.06% between 30 and 200 °C due to removal of physisorbed water) within the entire temperature range, indicating that it is thermally stable. As for MnO_2 and OMS-2, the contents of physisorbed water are ca. 3.85% and 1.64%, respectively. In the 200–400 °C range, an obvious weight loss of about 5.8% is observed over MnO_2, mainly due to the removal of chemisorbed water [24]. On the contrary, the weight loss in the 200–400 °C range observed over OMS-2 material is only ca. 0.65%. The results suggest that compared with MnO_2, OMS-2 is more hydrophobic and the adsorption of organic compounds is more favorable on OMS-2. The major weight loss of OMS-2 and MnO_2 occurs between 400 and 680 °C and there is a less remarkable one above 680 °C (Figs. 2(b) and (c)); the former is due to the reduction of MnO_2 to Mn_2O_3 and the latter is due to the transformation of Mn_2O_3 to Mn_3O_4 [22]. It is worth pointing out that the weight losses above 680 °C occur at different temperatures with that of OMS-2 lower than that of MnO_2 by ca. 90 degrees. Referring to the small weight loss of Mn_3O_4 (about 0.06%, Fig. 2a), it is apparent that there is thermal decomposition of MnO_2 and OMS-2 to Mn_3O_4. The weight losses due to release of lattice oxygen from OMS-2 and MnO_2 are 7.55% and 10.38%, respectively. Clearly, there are plenty of lattice oxygen species in OMS-2 and MnO_2 that would become mobile upon thermal excitation.

Table 1
Physical characteristics of catalysts.

Sample	Particle size[a] (nm)	Surface area (m^2/g)		Pore volume (cm^3/g)	
		S_{BET}[b]	S_{EXT}[b]	V_{total}[c]	V_{mic}[c]
Fresh OMS-2	11.9	71.8	67.2	0.359	0.003
Used OMS-2	11.3	70.5	66.7	0.359	0.002

[a] Particle size: calculated from Scherrer's equation.
[b] S_{BET}: BET surface area. S_{EXT}: external surface area.
[c] V_{total}: total pore volume. V_{mic}: micropore volume.

The O_2-TPD profiles of commercial Mn_3O_4, OMS-2, and commercial MnO_2 are shown in Fig. 3A There is only one small peak at 530 °C in the profile of Mn_3O_4, which is attributable to the desorption of chemisorbed oxygen species (Fig. 3A(a)). Over OMS-2, there are two major peaks (one at 490 °C and the other at 670 °C), and there is a small shoulder at 320–460 °C (Fig. 3A(b)). According to Genuino et al. [25] and Santos et al. [26], the shoulder peak can be ascribed to the desorption of chemisorbed oxygen, whereas the peaks at 490 and 670 °C can be attributed to the desorption of lattice oxygen due to the conversion of cryptomelane to Mn_2O_3 and that of Mn_2O_3 to Mn_3O_4, respectively, in agreement with the TGA results (Fig. 2b). Over commercial MnO_2, two major peaks at 520 (more intense) and 770 °C, and a small one at 580 °C are observed (Fig. 3A(c)). The peak at 520 °C is ascribed to desorption of surface oxygen species and labile oxygen species, about 30 °C higher than that of OMS-2 (at 490 °C). The other two peaks are due to desorption of lattice oxygen [25]. Comparing the O_2-TPD profiles of MnO_2 and OMS-2, the oxygen species of the former are thermally more stable than that of the latter. Luo et al. reported that for cryptomelane-type octahedral molecular sieves, desorption of oxygen could lead to the formation of oxygen vacancies which might be active sites for catalytic oxidation [27]. Wang and Li demonstrated that the catalysts with weaker Mn—O bonds are usually higher in lattice defects and labile lattice oxygen, and exhibit better performance [28]. It was confirmed that labile lattice oxygen has a promotional effect on catalytic activity [27,28]. Based on the TGA and O_2-TPD results, it

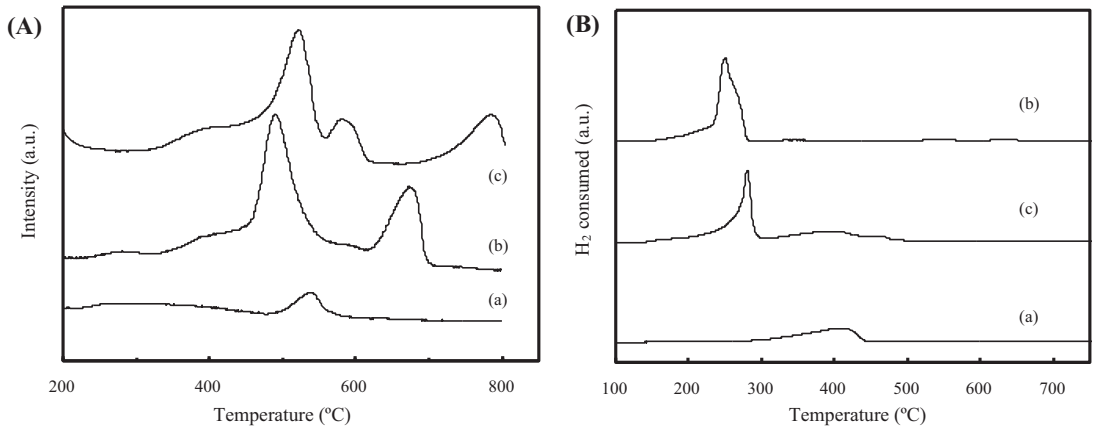

Fig. 3. (A) O_2-TPD and (B) H_2-TPR profiles of (a) commercial Mn_3O_4, (b) OMS-2, and (c) commercial MnO_2.

is deduced that OMS-2 has high provision of lattice oxygen species that are dislodged from the framework.

Depicted in Fig. 3B are the H_2-TPR profiles of commercial Mn_3O_4, OMS-2, and commercial MnO_2. In the case of Mn_3O_4, there is only one weak band at 410 °C corresponding to the reduction of Mn_3O_4 to MnO. Over OMS-2, there is a broad profile of two overlapping peaks, corresponding to a two-step reduction process. Assuming that MnO is the final state in the reduction of OMS-2 Mn species [24], the component at lower temperature could be assigned to the reduction of MnO_2/Mn_2O_3 to Mn_3O_4, and that at higher temperature to the reduction of Mn_3O_4 to MnO [25]. As for MnO_2, there is one main band at 280 °C and a weak band at 400 °C. According to the results of Wang et al. [29] and Stobbe et al. [30], the reduction process could be reasonably divided into two steps: (I) $Mn^{4+} \rightarrow Mn^{3+}$ and (II) $Mn^{3+} \rightarrow Mn^{2+}$. It is obvious that compared with MnO_2 and Mn_3O_4, OMS-2 can be reduced at much lower temperatures. In other words, the Mn—O bonds of OMS-2 are relatively weaker and the Mn species in OMS-2 can be reduced more easily. The hydrogen consumption was calculated based on the area of the reduction peaks. Theoretically, the H_2 consumptions for the reduction of MnO_2 to Mn_3O_4 and that of Mn_3O_4 to MnO are 7.67 and 3.83 mmol/g, respectively. In the present study, the total H_2 consumption for OMS-2, MnO_2 and Mn_3O_4 are respectively 10.39, 13.29, and 4.74 mmol/g. The total H_2 consumptions of MnO_2 and Mn_3O_4 are quite close to the theoretical values. The results indicate that substantial amount of Mn^{4+} in MnO_2, and Mn^{4+} and Mn^{3+} in OMS-2 can be reduced to Mn^{2+} below 400 °C. Furthermore, the total amount of H_2 consumption detected over OMS-2 suggests a stage of mixed-valence. Being multi-valent is essential for electron transfer in a material, and hence the co-existence of various oxidation states of Mn in OMS-2 is important for electron transport. The efficiency of catalysts, especially those for redox reaction, is usually governed by their ability and tendency to cycle among the valence states of manganese.

3.2. Catalytic activity

To study the factors that influence *p*-chlorotoluene oxidation, several manganese compounds and a number of transition metal oxides were tested as catalysts. Table 2 lists the *p*-chlorotoluene conversion and selectivity to *p*-chlorobenzaldehyde, *p*-chlorobenzyl alcohol, and *p*-chlorobenzoic acids. In a blank run (without a catalyst) and over commercial Fe_2O_3, there is no conversion of *p*-chlorotoluene. It is known that cobalt oxide [5,11,31] and vanadium oxide [1,10] are excellent catalysts for C—H bond activation in the oxidation of *p*-chlorotoluene to *p*-chlorobenzaldehyde. We found that when Co_2O_3 and V_2O_5 are used as catalysts, *p*-chlorotoluene conversion reaches 49.7% and 41.1%, respectively, but selectivity to *p*-chlorobenzaldehyde is only 1.1% and 25.7%. In addition, the *p*-chlorotoluene conversion over Mn_3O_4 is only 26.5% while that over commercial MnO_2 is 54.5%, but selectivity to *p*-chlorobenzaldehyde is relatively low (44.1%). However, using the synthesized OMS-2, we achieve a *p*-chlorotoluene conversion of 86.0%, indicating that the as-synthesized OMS-2 is active for *p*-chlorotoluene oxidation in the adopted liquid-phase catalytic oxidation system. The selectivity to *p*-chlorobenzaldehyde and that to *p*-chlorobenzoic acids are 68.7% and 31.3%, respectively. The observations suggest that the OMS-2 is an appropriate catalyst for the *p*-chlorotoluene aerobic oxidation system, and the as-synthesized OMS-2 shows better catalytic activity than commercial MnO_2 and Mn_3O_4. Therefore, OMS-2 catalyst was adopted in the rest of the study to investigate the effects of reaction conditions on catalytic activity.

That catalytic activity is closely related to the physical and chemical properties of catalysts is known. Taking the TPD and TGA results into account, the catalytic activity of OMS-2 could be correlated with the nature of lattice oxygen. The abundance of lattice oxygen could be a reason why OMS-2 is high in *p*-chlorotoluene conversion. In addition, the catalytic activity can be attributed to oxygen mobility: the higher the oxygen mobility, the better the activity [25,29]. With desorption and reduction of oxygen occurs at temperatures lower than those of MnO_2, it is considered that the OMS-2 catalyst is high in lattice oxygen mobility. For better understanding of the role of lattice oxygen on the catalytic properties of OMS-2, a series of OMS-2 differing in composition, morphology, and specific surface area were synthesized and examined for the liquid-phase catalytic

Table 2
Results of *p*-chlorotoluene oxidation over different catalysts.[a]

Entry	Catalyst	Conv. (mol%)	Product distribution (mol%)			
			PCB[b]	PCA[b]	PCBA[b]	Others
1	No catalyst	0	0	0	0	0
2	OMS-2	86.0	68.7	0	31.3	0
3	MnO_2	54.5	44.1	0	42.8	13.1
4	Mn_3O_4	26.5	45.1	0	36.2	18.7
5	$Mn(OAc)_2$	31.1	33.6	0.7	19	46.7
6	Co_2O_3	49.7	1.1	0.9	2.5	95.5
7	V_2O_5	41.1	25.7	0	7.6	66.7
8	Fe_2O_3	0	0	0	0	0

[a] Reaction conditions: catalyst = 50 mg, *p*-chlorotoluene = 1 mL, solvent (acetic acid) = 10 mL, water = 2 g, HBr (40 wt. %) = 0.02 g, oxygen flow rate = 50 mL/min, time = 10 h, temperature = 100 °C.
[b] PCB: *p*-chlorobenzaldehyde; PCA: *p*-Chlorobenzyl alcohol; PCBA: *p*-Chlorobenzoic acid.

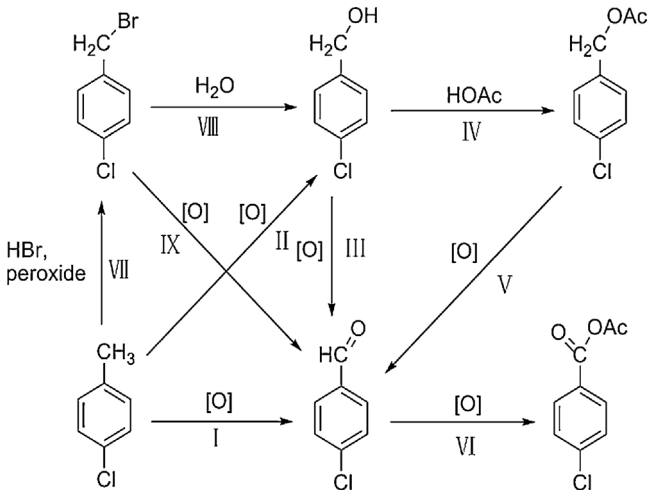

Fig. 4. Reaction network during the oxidation of *p*-chlorotoluene using metal/bromide catalysts [32].

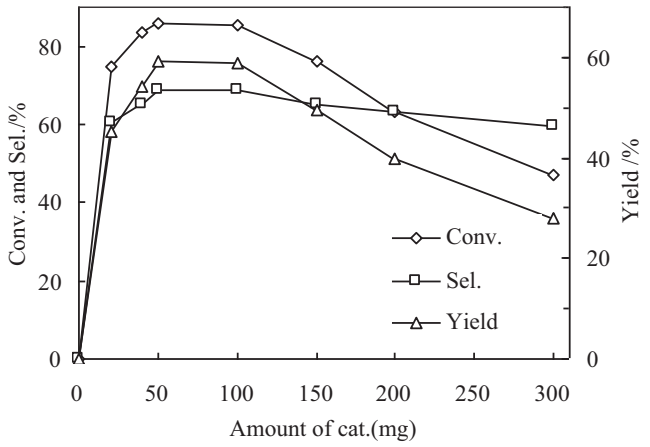

Fig. 6. Effect of catalyst amount on *p*-chlorotoluene oxidation (reaction conditions: substrate 1 mL, solvent 10 mL, HBr (40 wt.%) 0.02 g, water 2 g, oxygen flow rate 50 mL/min, time 10 h, temperature 100 °C).

oxidation of *p*-chlorotoluene. We find that the catalysts higher in oxygen mobility and with more lattice oxygen species exhibit better catalytic activity. The related results will be published in the near future.

3.3. Effect of reaction conditions

3.3.1. Effect of water addition

The sequence of reactions that occurs during metal/bromide autoxidation of *p*-chlorotoluene is given in Fig. 4 [32]. The effect of water addition on *p*-chlorotoluene conversion is depicted in Fig. 5 One can see that water can promote the oxidation of *p*-chlorotoluene, and there is a point that water would be in excess and the catalysis is inhibited. In the absence of water, the autoxidation of *p*-chlorotoluene takes place at very low rate. It is plausible that under mild conditions, the extent of peroxide decomposition for the generation of radicals is low. After the addition of a small quantity of water, there is enhanced radical concentration because the protons of water molecules interact with the peroxide molecules, facilitating the splitting of O—O bond of H-bonded peroxide complexes [32]. When water is in excess, the concentration of active water starts to decrease due to self-association, and there is decline in radical production and diminution of overall reaction rate. Ultimately, water appears as a separate phase, and the rate drops to almost that of the initial low value [33].

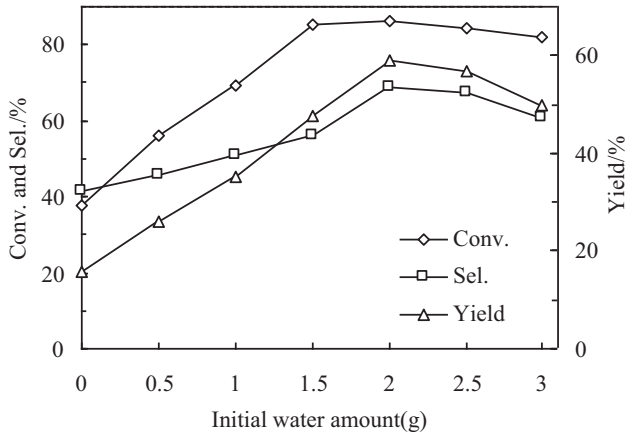

Fig. 5. Effect of water addition on *p*-chlorotoluene oxidation (reaction conditions: catalyst 50 mg, substrate 1 mL, solvent 10 mL, HBr (40 wt.%) 0.02 g, oxygen flow rate 50 mL/min, time 10 h, temperature 100 °C).

As shown in Fig. 5, when the amount of water added initially to the system is lower than 2 g, there is enhancement of catalytic activity. When the initial water amount exceeds 2 g, there is decline in *p*-chlorotoluene conversion plausibly due to the strong deactivation effect of water on reaction VI (Fig. 4). In parallel to the increase of *p*-chlorotoluene conversion, there is rise of *p*-chlorobenzaldehyde selectivity. Also, when the initial water amount exceeds 2 g, there is decrease in *p*-chlorobenzaldehyde selectivity. It is because with obvious decrease of catalytic activity, it is difficult for *p*-chlorobenzyl alcohol and *p*-chlorobenzyl acetate to be further oxidized to *p*-chlorobenzaldehyde (reactions III and V, Fig. 4). Moreover, an excessive amount of water may have an inhibition effect on reaction I (Fig. 4). Taking *p*-chlorobenzaldehyde yield into consideration, the most suitable initial water amount should be 2 g in the present reaction system.

3.3.2. Effect of catalyst amount

The catalyst amount was varied between zero and 300 mg. In Fig. 6, one can see that even a small amount (20 mg) of as-synthesized OMS-2 can lead to significant *p*-chlorotoluene conversion (74.8%). Between catalyst amounts of 40 and 100 mg, *p*-chlorotoluene conversion varies only slightly from 83.4% to 85.4%. The phenomenon suggests that the conversion is limited by the availability of dissolved oxygen which is rather constant under the adopted reaction conditions [34]. Furthermore, we studied the effect of mass transfer limitation by varying the stirring rate from 500 to 1200 rpm. We observed that there is little change in conversion as well as in selectivity. The results suggest that mass transfer limitation has little effect on the reaction under the adopted conditions.

However, when the amount of catalyst is above 100 mg, there is significant decline in *p*-chlorotoluene conversion. It was pointed out by Black [35] that transition metal salts or some biomimetic catalytic systems function as catalysts at low loadings but as inhibitors at high loadings. If more radicals are formed due to higher loading of catalyst, there is actually a decline in activity due to self-termination of radicals. It is believed that due to the combination of radicals, there is decline in radical concentration and hence less conversion of *p*-chlorotoluene (Fig. 6). The variation of catalyst amount between 40 and 300 mg does not affect the selectivity to *p*-chlorobenzaldehyde significantly (59.7–68.9%). In terms of maximum *p*-chlorobenzaldehyde yield, a catalyst amount of 50 mg is

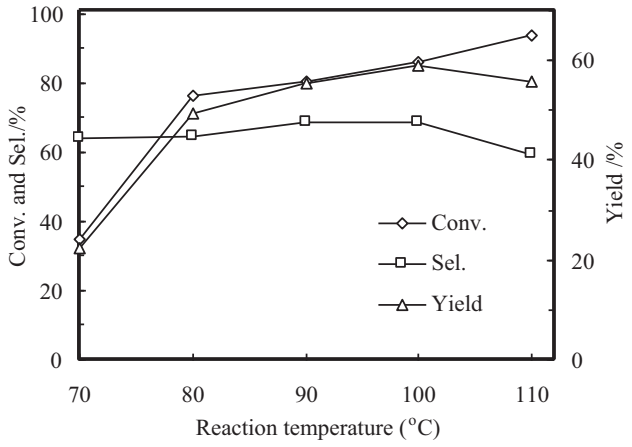

Fig. 7. Effect of reaction temperature on *p*-chlorotoluene oxidation (reaction conditions: catalyst 50 mg, substrate 1 mL, solvent 10 mL, HBr (40 wt.%) 0.02 g, water 2 g, oxygen flow rate 50 mL/min, time 10 h).

the most suitable for this liquid-phase *p*-chlorotoluene oxidation system.

3.3.3. Effect of reaction temperature

The influence of reaction temperature on the conversion of *p*-chlorotoluene was investigated from 70 to 110 °C (Fig. 7). It can be seen that the yield of *p*-chlorobenzaldehyde comes to a maximum at 100 °C. A rise of temperature above 100 °C (e.g. 110 °C which is close to the boiling point) results in poor yield of *p*-chlorobenzaldehyde. The phenomenon is a result of low O_2 solubility in the liquid phase at such a high temperature [36].

3.3.4. Effect of reaction time

The change of *p*-chlorotoluene, *p*-chlorobenzaldehyde, and *p*-chlorobenzoic acid in the reaction system with time was investigated (Fig. 8) One can see rapid rise of *p*-chlorobenzaldehyde selectivity whereas the rise of selectivity to *p*-chlorobenzoic acid is moderate. Simultaneously, the selectivity to *p*-chlorobenzyl bromide and *p*-chlorobenzyl alcohol decreases rapidly due to the corresponding consecutive reactions VIII, IX and III, IV (Fig. 4). With prolonged reaction, there is constant rise of *p*-chlorobenzaldehyde concentration, leading to further oxidation and the formation of *p*-chlorobenzoic acid (reaction VI, Fig. 4) as reflected in the decrease

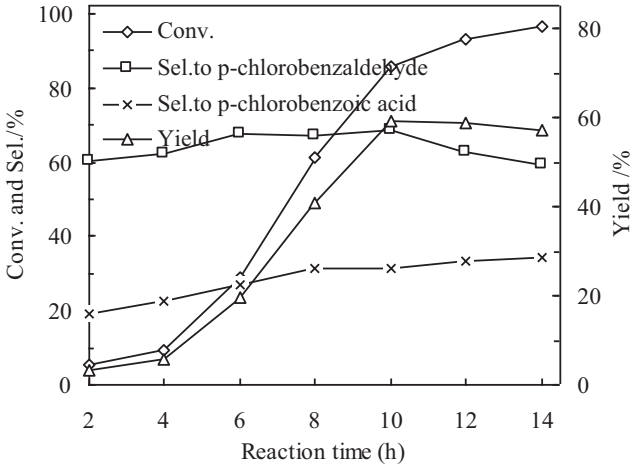

Fig. 8. Effect of reaction time on *p*-chlorotoluene oxidation (reaction conditions: catalyst 50 mg, substrate 1 mL, solvent 10 mL, HBr (40 wt.%) 0.02 g, water 2 g, oxygen flow rate 50 mL/min, temperature 100 °C).

of *p*-chlorobenzaldehyde selectivity and rise of selectivity to *p*-chlorobenzoic acid.

3.4. Leaching experiments and catalyst stability

To verify that there was no leaching of catalyst during the reaction, OMS-2 was used under the adopted conditions but removed after 4 h, and the mixture was left to react for another 10 h. It was found that there is almost complete suspension of reaction upon OMS-2 removal. In other words, the leach of catalyst into the liquid phase is insignificant.

Tests were conducted to investigate the recyclability of the OMS-2 catalyst. After each run, the catalyst was filtered out and washed several times with acetone or alcohol before being dried at 110 °C overnight. Across the four runs, there is only insignificant change in *p*-chlorotoluene conversion and *p*-chlorobenzaldehyde selectivity (Fig. S2). The XRD patterns (Fig. 1b) and N_2 adsorption/desorption isotherms (Table 1) of used catalysts indicate that the main characteristics of the catalyst are preserved during the four cycles of oxidation reaction.

3.5. Possible reaction mechanism

The liquid-phase catalytic oxidation of *p*-chlorotoluene to *p*-chlorobenzoic acid in an acetic acid media is typical of aromatic hydrocarbon oxidation processes, which belongs to the kind of classical free-radical chain reactions. Researchers such as Kamiya [37], Suresh et al. [38], and Wang et al. [39] studied the mechanism of liquid-phase catalytic oxidation of aromatic hydrocarbons for many years. The initiation mechanism is predominantly hydrogen abstraction from methyl groups by bromine atoms. The Mn and/or Co ions oxidize the resulted bromine ions to bromine atoms thus ensuring the availability of bromine atoms for initiation.

We investigated the oxidation reaction of *p*-chlorotoluene with HBr in N_2, and obtained only 10.8% conversion. The finding corroborates that the aerobic benzyl alcohol oxidation over OMS-2 catalysts proceeds according to a Mars-van Krevelen mechanism [16,40]. Thus, the conversion observed in the N_2 stream can be explained by substrate oxidation with oxygen supplied from the solid manganese-oxide-based OMS-2 catalyst. Without further supply of gas-phase oxygen to reoxidize the catalyst, the reaction slows down and essentially stops. According to the results of this study and the mechanism depicted in literatures, we propose a mechanism for the liquid-phase catalytic oxidation of *p*-chlorotoluene to *p*-chlorobenzaldehyde over OMS-2. When the oxidation reaction of *p*-chlorotoluene is performed without HBr, there is no *p*-chlorotoluene conversion. We hence deduce that at the beginning the Mn(IV) ions oxidize bromine ions to bromine radical thus ensuring the availability of bromine radicals for initiation (see Eq. (1)) [41].

$$\mathrm{Mn(IV) + Br^- \rightarrow Mn(III) + Br^\bullet} \quad (1)$$

The $Br^\bullet$ radical initiates the oxidation of *p*-chlorotoluene by hydrogen abstraction according to the following radical reaction:

$$\mathrm{Br^\bullet + \textit{p}\text{-Cl-Ph-CH_3} \rightarrow \textit{p}\text{-Cl-Ph-CH_2^\bullet} + H^+ + Br^-} \quad (2)$$

("Ph" denotes benzene ring and "*p*" denotes the para-substituted group). The generated *p*-Cl-Ph-$CH_2^\bullet$ radical has high reactivity and combines with molecular oxygen to generate *p*-CH_3-Ph-$CH_2O_2^\bullet$ radical by the reaction:

$$\mathrm{\textit{p}\text{-Cl-Ph-CH_2^\bullet} + O_2 \rightarrow \textit{p}\text{-Cl-Ph-CH_2O_2^\bullet}} \quad (3)$$

Then the following radical reaction occurs:

$$\mathrm{\textit{p}\text{-Cl-ph-CH_2O_2^\bullet} + Mn(III) + H^+ \rightarrow \textit{p}\text{-Cl-Ph-CHO} + Mn(IV) + H_2O} \quad (4)$$

The major chain termination reactions are that between two radicals [42]. At early stage of reaction, we detected a higher concentration of *p*-chlorobenzyl bromide by GCMS, but at the last period of the reaction *p*-chlorobenzyl bromide disappeared, via the corresponding consecutive reactions VIII, IX (Fig. 4). We hence deduce that $Br^{\cdot}$ radicals have an important role to act in chain initiation and propagation [33,42]. The following reaction between $Br^{\cdot}$ radical and other radicals are considered as the chain termination reaction.

$$Br^{\bullet} + p\text{-Cl-Ph-}CH_2^{\bullet} \rightarrow p\text{-Cl-Ph-}CH_2Br \quad (5)$$

The aromatic aldehyde group also can be oxidized to the corresponding peroxide radical $RCO_3^{\cdot}$ in the same manner as that of methyl group, and then reacts with low valance metal to generate aromatic peracid RCOOOH [43]. The reactions are as follows:

$$Br^{\bullet} + p\text{-Cl-Ph-CHO} \rightarrow p\text{-Cl-Ph-}CO^{\bullet} + H^{+} + Br^{-} \quad (6)$$

$$p\text{-Cl-Ph-}CO^{\bullet} + O_2 \rightarrow p\text{-Cl-Ph-}CO_3^{\bullet} \quad (7)$$

$$p\text{-Cl-Ph-}CO_3^{\bullet} + Mn(III) + H^{+} \rightarrow p\text{-Cl-ph-COOOH} + Mn(IV) \quad (8)$$

The reducibility of aldehyde group is strong and the following self-catalyzed reaction between aldehyde group and aromatic peracid occurs to generate aromatic acid [41]:

$$p\text{-Cl-Ph-COOOH} + p\text{-Cl-Ph-CHO} \rightarrow 2p\text{-Cl-Ph-COOH} \quad (9)$$

Besides the generation of aromatic acid via Baeyer-Villiger reaction (reaction Eq. (9)), peroxyacid reacts with Mn(III) to give the aromatic acid according to the following reaction:

$$p\text{-Cl-Ph-COOOH} + 2Mn(III) + 2H^{+} \rightarrow p\text{-Cl-Ph-COOH} + 2Mn(IV) + H_2O \quad (10)$$

4. Conclusion

Liquid-phase catalytic oxidation of *p*-chlorotoluene with molecular oxygen using synthesized OMS-2 octahedral molecular sieve as catalyst results in promising conversion and selectivity in the adopted atmospheric reflux system. The TPD and TGA results confirm that there is a large amount of highly mobile lattice oxygen in OMS-2, and the activation of *p*-chlorotoluene is promoted as a result. Under optimum conditions, an 86.0% conversion of *p*-chlorotoluene along with 68.7% selectivity to *p*-chlorobenzaldehyde is obtained. The OMS-2 catalyst shows promising reusability and can be recycled. A free-radical reaction mechanism is proposed. The OMS-2 catalyst with such activity, selectivity, and recyclability opens up new possibilities for the conversion of aromatic hydrocarbons to the corresponding aldehydes with O_2 in liquid-phase atmospheric systems.

Acknowledgments

The project was financially supported by NSFC (Grant Nos. 21273067, U1162109, 20873038), the program for New Century Excellent Talents in Universities (NCET-10-0371), Program for Changjiang Scholars and Innovative Research Team in University (IRT1238), Hunan Provincial Natural Science Foundation of China (10JJ1003), and the Fundamental Research Funds for Central Universities. C.T. Au thanks the Hunan University for an adjunct professorship.

Y.Q. Deng and T. Zhang contributed equally.

Appendix A. Supplementary data

Supplementary data associated with this article can be found, in the online version, at http://dx.doi.org/10.1016/j.apcata.2013.07.015.

References

[1] R.A. Sheldon, H. Van Bekkum, Fine Chemicals through Heterogeneous Catalysis, Wiley-VCH, Weinheim, 2001.
[2] P. Anastas, J. Warner, Green Chemistry: Theory Practice, Oxford University Press, New York, 1998.
[3] F.M. Bautista, D. Luna, J. Luque, J.M. Marinas, J.F. Sánchez-Royo., Appl. Catal. A 352 (2009) 251–258.
[4] F. Konietzni, U. Kolb, U. Dingerdissen, W.F. Maier, J. Catal. 176 (1998) 527–535.
[5] J. Wang, H. Fang, Y. Li, J. Li, Z. Yan, J. Mol. Catal. A: Chem. 250 (2006) 75–79.
[6] YooF J.S., Appl. Catal., A 135 (1996) 261–271.
[7] H. Borchert, T. Gerdau, J. Weiguny, US Patent 5,648,551 (1997).
[8] F.M. Bautista, J.M. Campelo, D. Luna, J. Luque, J.M. Marinas, Catal. Today 128 (2006) 183–190.
[9] F.M. Bautista, J.M. Campelo, D. Luna, J. Luque, J.M. Marinas, Appl. Catal., A 325 (2007) 336–344.
[10] A.P. Singh, T. Selvam, Appl. Catal., A 143 (1996) 111–124.
[11] R. Fatemeh, H.C. James, K. Babak, J.M. Duncan, Org. Biomol. Chem. 3 (2005) 725–726.
[12] T. Punniyamurthy, S. Velusamy, J. Iqbal, Chem. Rev. 105 (2005) 2329–2363.
[13] Fabrizio.F C., J. Chem. Technol. Biotechnol. 85 (2010) 1175–1183.
[14] D.W. Liu, B.B. Garcia, Q.F. Zhang, Q. Guo, Y.H. Zhang, S. Sepehri, G.Z. Cao, Adv. Funct. Mater. 19 (2009) 1015–1023.
[15] Z.S. Wu, W. Ren, D.W. Wang, F. Li, B. Liu, H.M. Cheng, ACS Nano 4 (2010) 5835–5842.
[16] Y.C. Son, V.D. Makwana, A.R. Howell, S.L. Suib, Angew. Chem. Int. Ed. 40 (2001) 4280–4283.
[17] S.L. Suib, Acc. Chem. Res. 41 (2008) 479–487.
[18] M.A. Peluso, L.A. Gambaro, E. Pronsato, D. Gazzoli, H.J. Thomas, J.E. Sambeth, Catal. Today 133 (2008) 487–492.
[19] V.D. Makwana, Y.C. Son, A.R. Howell, S.L. Suib, J. Catal. 210 (2002) 46–52.
[20] G. Leofanti, M. Padovan, G. Tozzola, B. Venturelli, Catal. Today 41 (1998) 207–219.
[21] X. Tang, Y. Li, J. Chen, Y. Xu, W. Shen, Microporous Mesoporous Mater. 103 (2005) 250–256.
[22] J. Luo, Q. Zhang, J. Garcia-Martinez, S.L. Suib, J. Am. Chem. Soc. 130 (2008) 3198–3207.
[23] Z.M. Wang, S. Tezuka, H. Kanoh, Chem. Mater. 13 (2001) 530–537.
[24] H. Sun, S. Chen, P. Wang, X. Quan, Chem. Eng. J. 178 (2011) 191–196.
[25] H.C. Genuino, S. Dharmarathna, E.C. Njagi, M.C. Mei, S.L. Suib, J. Phys. Chem. C 116 (2012) 12066–12078.
[26] V.P. Santos, M.F.R. Pereira, J.J.M. Órfão, Figueiredo.F J.L., Appl. Catal., B 99 (2010) 353–363.
[27] J. Luo, Q. Zhang, A. Huang, S.L. Suib, Microporous Mesoporous Mater. 35–36 (2000) 209–217.
[28] R. Wang, J. Li, Environ. Sci. Technol. 44 (2010) 4282–4287.
[29] F. Wang, H. Dai, J. Deng, G. Bai, Y. Liu, K. Ji, Environ. Sci. Technol. 46 (2012) 4034–4041.
[30] E.R. Stobbe, B.A. Boer, J.W. Geus, Catal. Today 47 (1999) 161–167.
[31] A. Hu, C. Lu, B. Li, Huo.F T., Ind. Eng. Chem. Res. 45 (2006) 5688–5692.
[32] W. Partenheimer, J. Mol, Catal. A: Chem. 206 (2003) 105–119.
[33] W. Partenheimer, Adv. Synth. Catal. 346 (2004) 297–306.
[34] A.R. Li, S.W. Tang, P.H. Tan, C.J. Liu, B. Liang, J. Chem. Eng. Data 52 (2007) 2339–2344.
[35] J.F. Black, J. Am. Chem. Soc. 100 (1978) 527–535.
[36] N. Takeo, I. Toshiyuki, M. Masatoshi, I. Takatoshi, M. Takumi, Tetrahedron Lett. 51 (2010) 2225–2227.
[37] Y. Kamiya, J. Catal. 33 (1974) 480–485.
[38] A.K. Suresh, M. Sharma, T. Sridhar, Ind. Eng. Chem. Res. 39 (2000) 3958–3997.
[39] Q. Wang, Y. Zhang, Y. Cheng, X. Li, AIChE J. 54 (2008) 2674–2688.
[40] F. Schurz, J.M. Bauchert, T. Merker, T. Schleid, H. Hasse, R. Glaser, Appl. Catal., A 355 (2009) 42–49.
[41] P. Raghavendrachar, S. Ramachadran, Ind. Eng. Chem. Res. 31 (1992) 453–462.
[42] M. Hronec, Z. Hrabe, Ind. Eng. Chem. Prod. Res. Dev. 25 (1986) 257–261.
[43] L.J. Wang, X. Li, G. Xie, Y.W. Cheng, J. Siman, J. Chem. Ind. Eng. 54 (2003) 946–952.